On the Nucleation of Graphite in Lamellar Graphite Cast Iron

G. Alonso
IK-4 Azterlan, Durango, Spain

D.M. Stefanescu
The Ohio State University, Columbus, OH and The University of Alabama, Tuscaloosa, AL.

P. Larrañaga, E. De la Fuente
IK-4 Azterlan, Durango, Spain

R. Suarez
IK-4 Azterlan and Veigalan Estudio, Durango, Spain

ABSTRACT

Extensive research on graphite nucleation in lamellar graphite irons was conducted over the years, with many theories, more or less rooted in experimental facts, being formulated. This work is a pursuit of the same goal- understanding nucleation of graphite. To this purpose, quenching experiments at successive stages during solidification of gray cast iron with various sulfur and titanium levels have been carried out. The objective is to elucidate the effect of these elements on the nucleation of graphite on its lamellar and superfine morphology.

Scanning electron microscopy was carried on to analyze the evolution of graphite as a function of fraction solid. The correlation between the percentage of sulfur and the main mechanisms of nucleation was established. It is confirmed that at S levels as low as 0.02wt% graphite nucleates mostly at the austenite liquid interface on carbon-rich regions in the liquid. At sulfur levels higher than 0.02wt%, graphite nucleates mostly on MnS inclusions. At 0.02wt% S both mechanisms are possible. In the case of superfine graphite, titanium carbides were also identified as possible nucleation sites.

Keywords: lamellar graphite iron, superfine interdendritic graphite, nucleation

INTRODUCTION

Gray cast iron, which acquired its name from the color of its fracture, is characterized by free carbon in the shape of lamellar (flake) graphite in the microstructure. The amount, shape, size and distribution vary within wide limits. In general, gray iron castings have little shrinkage and low contraction during solidification (≈ 1%), and are characterized by good machinability and castability, excellent corrosion resistance, but limited tensile strength and low elongations (<0.6%).

The ASTM standard A-247 classifies graphite shape in five categories: 1) Type-A graphite (LAG), which normally appears in inoculated gray iron when cooled at moderate speeds; the graphite lamellae are randomly oriented and uniformly distributed; 2) Type-B graphite, typical for grey irons with near eutectic composition; it appears as fine flake graphite at the center, surrounded by coarser flake graphite (rosette); 3) Type-C graphite found in hypereutectic grey irons as a result of solidification with minimum undercooling; it shows as thick and long grey sheets; 4) Type D graphite (LDG), formed in hypoeutectic or eutectic grey irons solidifying at high cooling rates; 5) Type-E graphite, promoted by either very low carbon equivalent or rapid solidification. Type-D and –E are also known as interdendritic or undercooled graphite.

Other intermediate shapes have been identified, such as coral graphite[1], a highly branched fibrous type of graphite that is different from either LDG or compacted graphite (e.g. Fig. 1a[2]), and superfine interdendritic graphite (SIG) (Fig. 1b), which is short and stubby, obtained through 0.3-0.4%Ti addition to low sulfur (<0.01%S) irons[3]. This graphite allows obtaining tensile strength exceeding 300MPa without a significant increase in hardness.[4]

The addition of titanium is directly related to the improvement of the mechanical properties. It is still not clear if this is because of increased austenite fraction, or graphite shape change, or both. Okada [5] suggested that Ti additions resulting in the formation of TiC produce low carbon regions at the solid/liquid (S/L) interface which favor nucleation of austenite. According to Wilford and Wilson[6], Ti reacts with N producing TiN or Ti(CN) that can act as nuclei for the solidification of primary austenite. However, the effect of Ti on graphite may not be related to graphite nucleation[7,8] but to graphite growth.

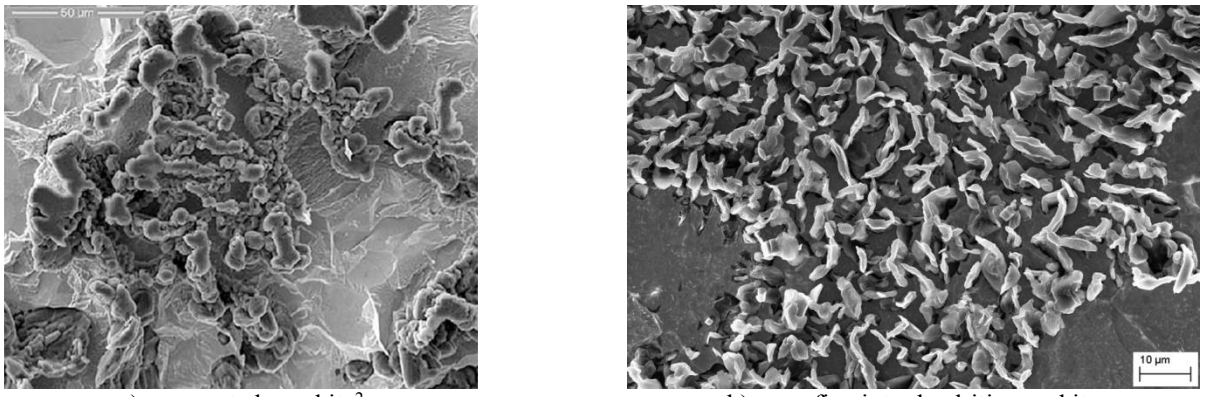

a) compacted graphite[2] b) superfine interdendritic graphite

Fig. 1. Images of the intermediate shapes.

Table 1. Chemical Composition (Mass %) of Experimental Cast Irons

Heat	Graphite	C	Si	CE	Mn	P	S	Ti	Mn/S
Q1SIG	LDG,SIG	2.94	1.92	3.50	0.58	0.022	0.011	0.180	52.7
Q2SIG	SIG	3.10	1.85	3.64	0.53	0.021	0.011	0.320	48.2
Q3LDG	LDG	3.07	1.91	3.59	0.57	0.014	0.011	0.014	51.8
Q4LDG	LDG	3.07	1.91	3.60	0.55	0.015	0.028	0.013	19.6
Q5LAG	LAG	3.02	1.90	3.55	0.53	0.019	0.120	0.013	4.4

The sulfur-titanium interaction on graphite nucleation is not completely understood. It is known that at relatively high sulfur content, manganese sulfide particles are formed, and act as nucleation sites for graphite precipitation[9–11]. The effect of sulfur on graphite shape depends on its content, with higher contents promoting type-A graphite[12]. At sulfur contents lower than 0.02wt% interdendritic graphite is to be expected because of the higher undercooling associated with lower sulfur.

The goal of this paper is to further understand the role of titanium in refining the graphite from LAG to LDG to SIG, and the influence of sulfur in the nucleation of graphite in grey cast irons.

EXPERIMENTAL STRATEGY

An in-depth SEM study was carried out on eutectic Fe-C-Si alloys produced from melts of commercial composition with various amounts of sulfur and titanium. The compositional range was designed such as to include irons with graphite ranging from lamellar LAG, to interdendritic LDG, and to superfine-interdendritic SIG.

MELTING AND CASTING

Five melts were produced in a 100 kg medium frequency induction furnace (250Hz, 100kw). For the first two melts (Q1SIG and Q2SIG) the charge consisted of 37kg of ductile iron returns and 13 kg of high purity pig iron. Ferromanganese (74.8%Mn, 2.13%Si, 5.49%C, 0.082%P and 17.3%Fe) and carburizer additions were made as needed. After superheating to 1500ºC, the iron was transferred into the pouring ladle. The heats had two different levels of titanium, 0.18% and 0.32%Ti, which was added as FeTi (72.3%Ti, 4.5%Al).

For the following three melts (Q3LDG, Q4LDG and Q5LAG) the original charge was the same as for the previous heats, but the titanium level was maintained constant at 0.014% (no Ti additions were made) and three levels of sulfur were used (0.011%, 0.028% and 0.120%).

From each melt, six standard (non-tellurium) thermal analysis cups were poured and the cooling curves were recorded. The system allowed recording of the cooling curve during quenching and cooling to room temperature. Inoculation was made directly in the cups through the addition of 0.2% of a commercial inoculant (62.6% Si, 0.22% Mg, 1.01% Al, 1.79% Ca, 5.96% Mn, 0.13% Ti, 6.77% Zr, 0.65% Ba).

The chemical analysis of all experimental irons and the graphite morphology is reported in Table 1. In addition to the elements listed in the table, the alloys contained 0.04%Cr, 0.01%Mo, 0.04%Ni, 0.04%Cu and less than 0.01%Al and 0.01%Mg. For the Ti containing irons the Mn/S ratio was relatively constant at about 50. For the no-Ti samples this ratio had three different levels.

The solidification of the iron in the cup was interrupted by quenching in brine at increasing times after the beginning of solidification, as shown as an example in Fig. 2. The purpose was to obtain information on the microstructure evolution at various stages during solidification. After cooling to room temperature, the cups were sectioned and prepared for metallographic examination.

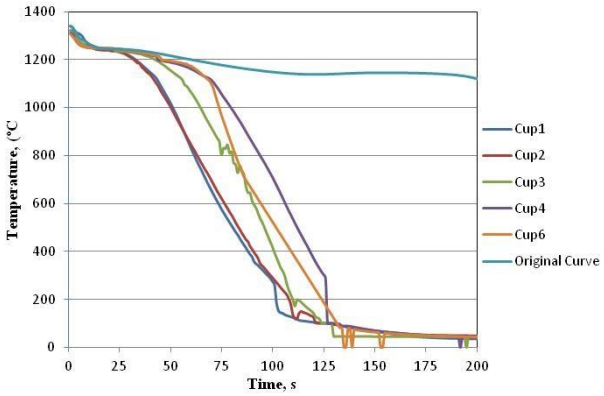

Fig. 2. Cooling curves obtained during the quenching experiments (Q4LDG).

CHARACTERIZATION

The fraction of the area, occupied by the solid after different solidification, times was measured through quantitative metallography techniques on color and Nital etched samples[13]. The liquid fraction includes cementite and ledeburite, while the solid fraction is formed of graphite, martensite, retained austenite and sometimes pearlite.

Optical metallography and SEM examination of graphite morphology was carried out on non-etched and deep-etched samples. Deep etching consists of 40 seconds etching with a solution of 40% nitric acid in water, followed by cleaning for five seconds in a solution of 50% clorhydric acid in water, all at ambient temperature. To find possible nucleation sites a SEM (0.8 nm resolution at 30 kV) in the STEM mode was used in combination with .an EDS detector with a resolution of 127 ev/mm^2.

EXPERIMENTAL RESULTS

In SIG irons (heats Q1SIG and Q2SIG) graphite nucleates at the austenite/liquid interface (γ/L) and then grow into the liquid (seen as carbides on the quenched microstructure) as exemplified in Fig. 3. If they have enough room, the austenite/graphite (γ/Gr) aggregates grow as spherical γ/Gr eutectic grains.

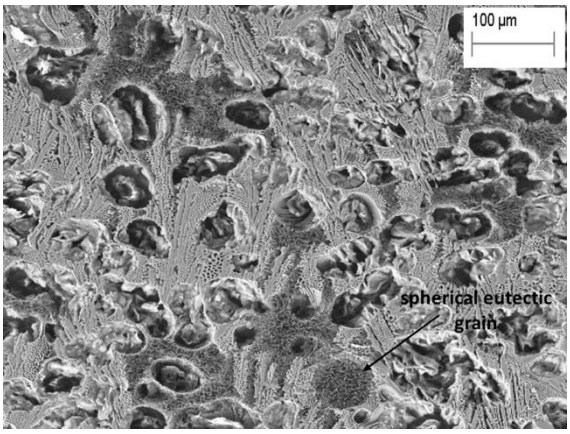

Fig. 3. Deep etching SEM image of a sample from heat Q2SIG (0.011% S, 0.32%Ti)

A significant number of titanium carbides (TiC) were observed in the microstructure (Fig. 4).

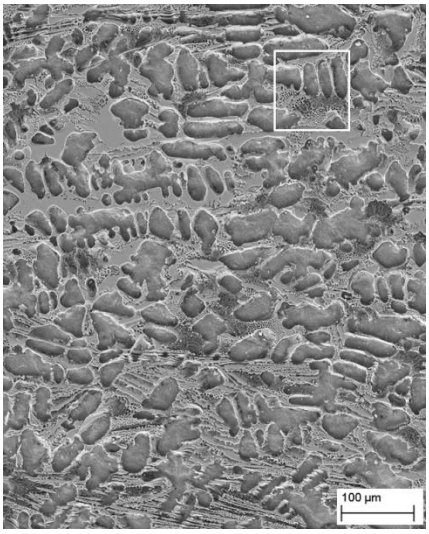

a) Lower magnification: graphite always in contact with austenite (f_S=0.66)

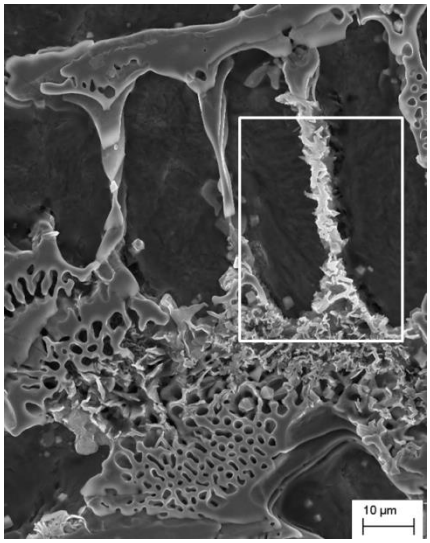

b) High magnification: graphite in contact with the liquid and austenite

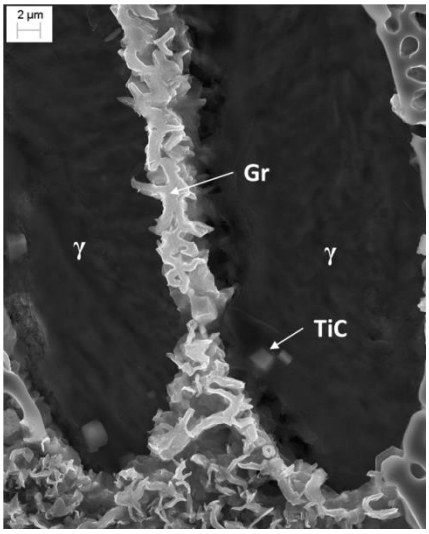

c) Higher magnification: austenite/graphite interface and TiC in the austenite

Fig. 4. Deep etching SEM images of the Q1SIG (0.011% S, 0.18%Ti).

Although they are mostly positioned in the austenite dendrites, there is evidence of their direct contact with the graphite (Fig. 5). As seen on Fig. 5b two graphite plates appear to originate from a cuboidal TiC carbide.

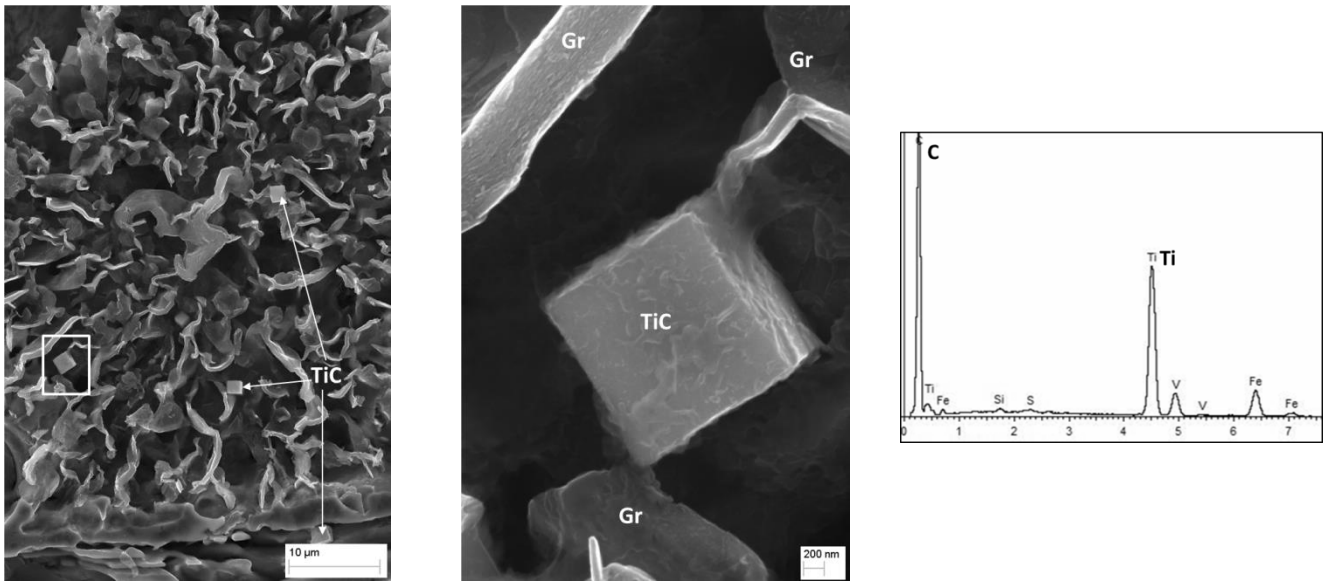

a) Low magnification: titanium carbides in the γ/Gr eutectic grain.

b) High magnification: TiC in contact with graphite lamellae.

c) WDX/SEM spectrum of the TiC.

Fig. 5. SEM images from heat Q1SIG (0.011%S, 0.18%Ti).

In an earlier paper[14], where numerous cuboidal TiC were found in contact with the graphite, the authors were uncertain that this was enough proof to accept the nucleation effect of the carbides. In light of these new findings it is reasonable to assume that cuboidal TiC carbides act as graphite nuclei.

In a previous study[15] (Ti,Mn)S inclusions were identified in addition to the cuboidal TiC in a high-S high-Ti (0.12% S, 0.36% Ti) iron (Fig. 6).

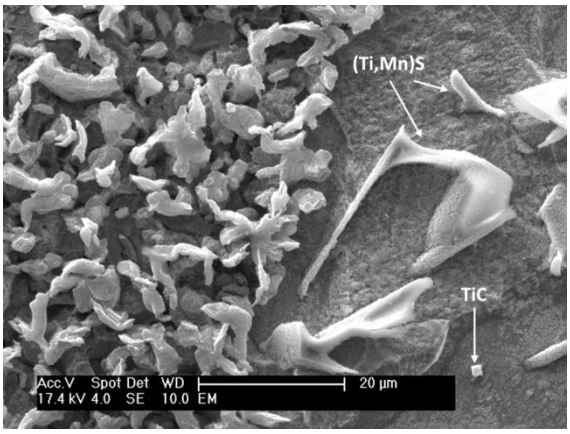

Fig. 6. TiC and (Ti,Mn)S inclusions in a 0.12% S, 0.36% Ti iron.[15]

Complex titanium inclusions were also observed in this work at the higher level of 0.32% Ti. They were first identified in standard, not etched, metallographic samples, and are of acicular morphology (see for example Fig. 7). As shown by the spectrum of these inclusions in Fig. 7c, they seem to contain some S and Mn. They will be referred to as TiCS needle-like carbides to distinguish them from the cuboidal TiC carbides. They are always in contact with the graphite. As the detailed SEM study did not find any MnS that could act as nuclei for the low sulfur SIG, it is possible that the TiCS inclusions serve as nuclei for graphite.

These needle-like carbides were not detected in a previous research[16] because after deep etching they can be confused with graphite. However, after their existence was documented from non-etched samples, it was possible to identify them on deep-etched SEM samples (Fig. 8). Fig. 8b shows a graphite plate in contact with TiCS needles at both ends. This could be construed as an argument in favor of the nucleation effect of TiCS carbide. However, it is also possible that the graphite plate has grown until obstructed by the two carbides.

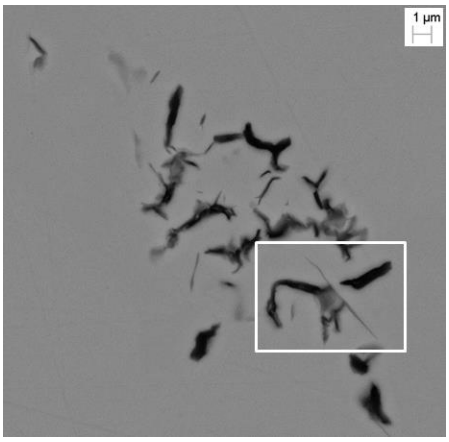

a) Low magnification: graphite and titanium carbides

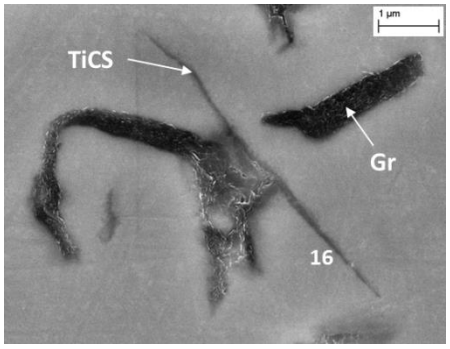

b) High magnification: TiCS needle

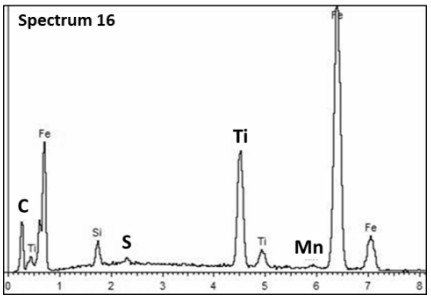

c) WDX/SEM spectrum of the TiCS needle

Fig. 7. SEM images from heat Q2SIG (0.011% S, 0.32%Ti) at f_S=0.52; not etched.

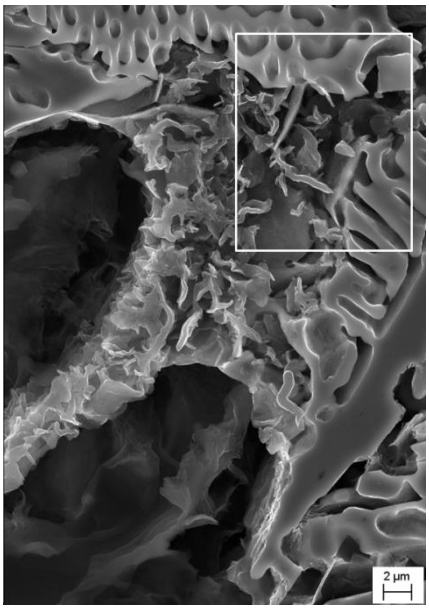

a) Low magnification view; f_S=0.55

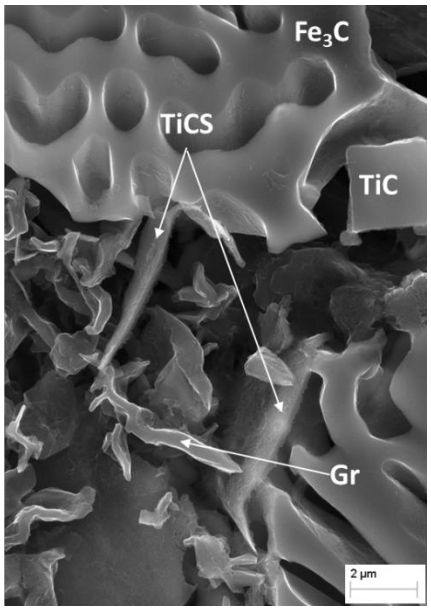

b) High magnification: graphite constrained between two TiCS needles

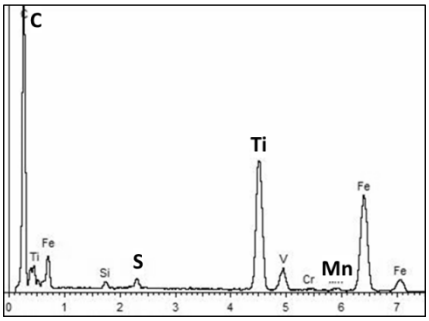

c) WDX/SEM spectrum of the TiCS needles

Fig. 8. Deep etching SEM images of iron Q2SIG (0.011% S, 0.32%Ti).

Once nucleated, the graphite grows in direct contact with the liquid as seen from Fig. 9, where the previous liquid is seen as iron carbide. The typical graphite morphology of SIG is illustrated in Fig. 10.

For the low-S no Ti addition heat Q3LDG the distribution of the graphite is similar to that in the SIG irons, but the morphology is different. The graphite plates are larger compared to that in SIG (Fig. 11b). No titanium carbides were observed in this iron. This was expected because of the low percentage of Ti (0.014%). Thus, it is reasonable to assume that nucleation occurs at the austenite/liquid interface (Fig. 11a) in regions enriched in carbon, because of carbon rejection by the austenite during solidification. This is in line with the fact that graphite additions are a potent nucleant in lamellar graphite iron.

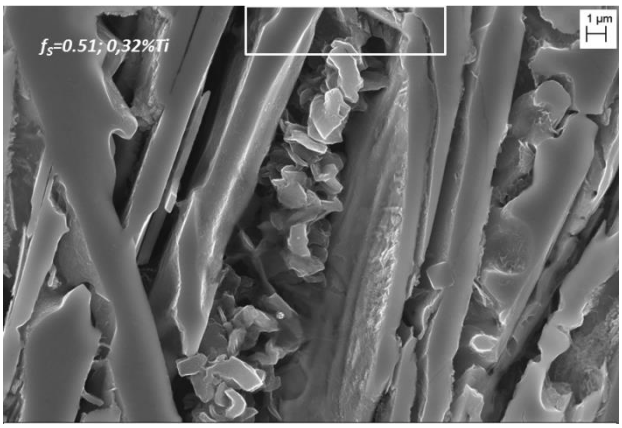

a) Low magnification: graphite surrounded by liquid; f_S=0.51.

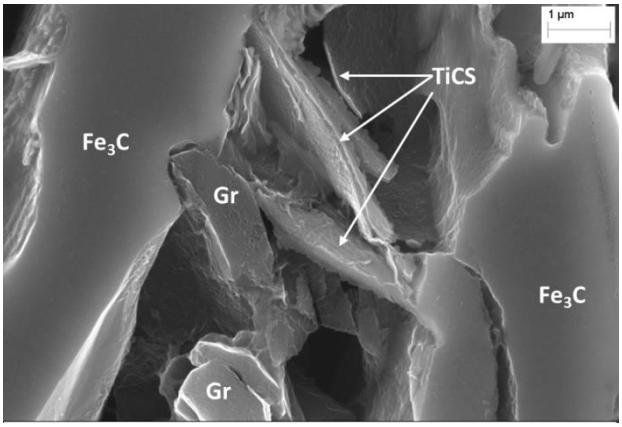

b) High magnification: graphite growing into the liquid.

Fig. 9. Deep etching SEM images of iron Q2SIG (0.011% S, 0.32%Ti).

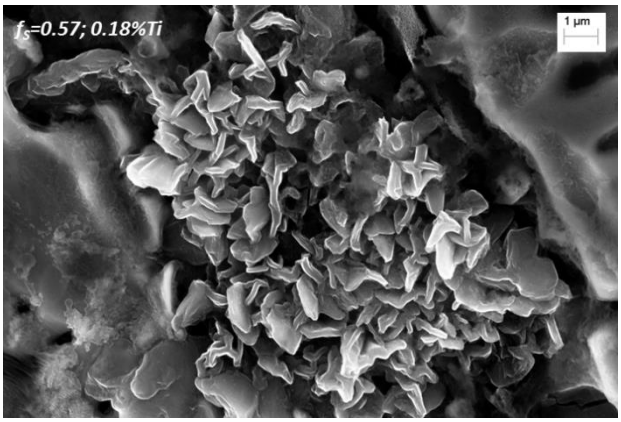

Fig. 10. Graphite morphology in heat Q1SIG (0.011%S, 0.18% Ti).

The morphology of the graphite in the medium sulfur (0.028%S) heat Q4LDG is similar to that in heat Q3LDG that is type-D, but the graphite is slightly larger, with a more chaotic distribution and with more varied shapes. Again graphite nucleates at the austenite/liquid interface, but also sometimes on MnS, as shown as an example in Fig. 12. Although the MnS particle itself is not visible, the spectrum signals its presence under the surface of the metallographic sample. Also, graphite growing in contact with the liquid is clearly seen. While most of the time the growth mechanism for graphite is plate stacking, some examples of helical growth were also found (Fig. 13).

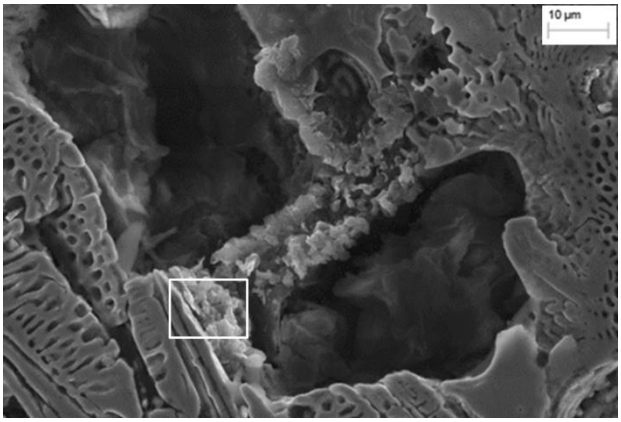

a) Growth of graphite at the γ/L interface

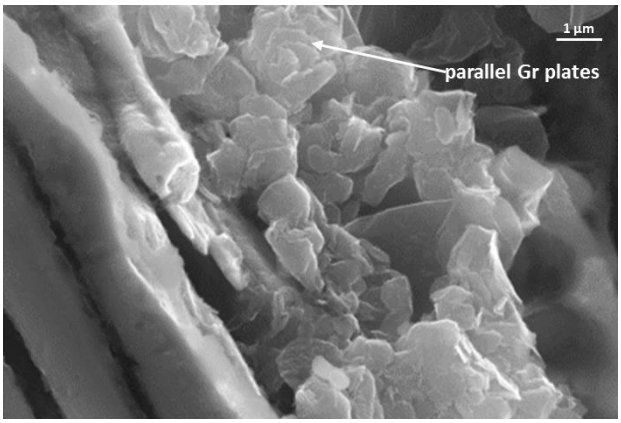

b) Higher magnification: growth of graphite

Fig. 11. Early solidification for the low-sulfur no-titanium addition iron Q3LDG (0.011% S, 0.014% Ti).

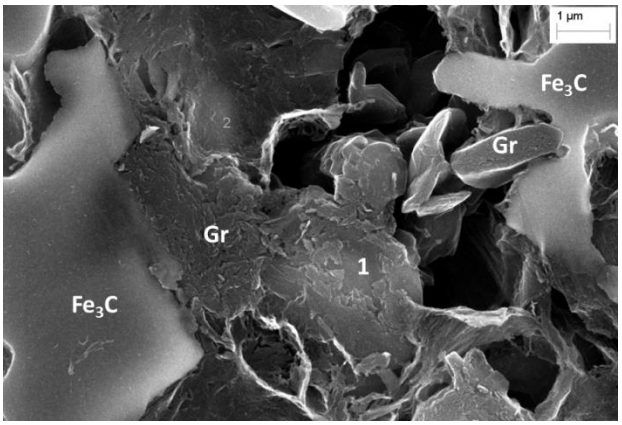

a) Gr nucleation on MnS and growth of the graphite in contact with the liquid.

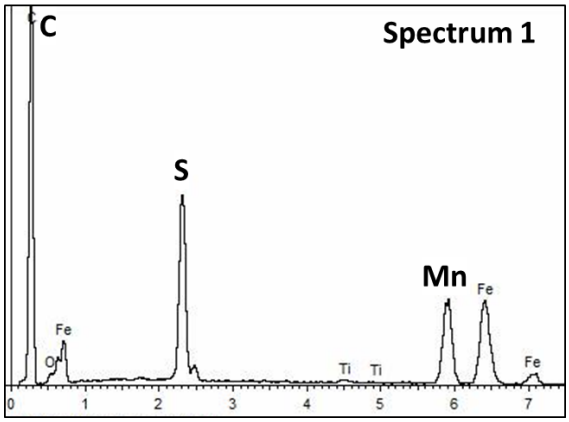

b) WDX/SEM spectrum of the subsurface MnS

Fig. 12. Early solidification (f_s=0.44) for the medium-sulfur no-titanium iron Q4LDG (0.028% S, 0.013% Ti).

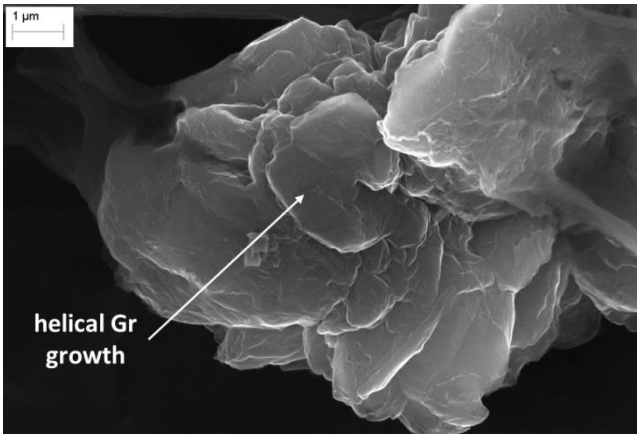

Fig. 13. Helical growth of LDG in heat Q4LDG (0.028% S, 0.013% Ti).

The last heat, Q5LAG, which is high in sulfur (0.12% S), exhibits graphite with a totally different morphology: type-A, more uniformly distributed, with higher aspect ratio and less roundness. Numerous MnS inclusions were observed. Not all MnS inclusions are graphite nuclei (Fig. 14a). When they are, the graphite envelops the MnS nuclei and then starts branching (Fig. 14c). Some complex oxy-sulfides of Zr, Al, Mg, Mn and Ca were found as nuclei of the MnS, as shown in Fig. 15. The source of these elements is probably the inoculant. The ZrO_2 (melting point 2715ºC, free energy of formation -195 kcal/gfw) and the MgO (free energy of formation -230 kcal/gfw) are the likely candidates to form in the melt. The MnS inclusions exhibit a variety of shapes, from polygonal to plates (Fig. 16).

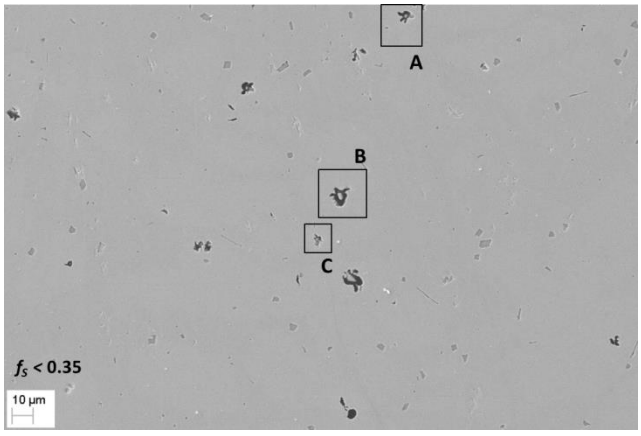

a) Low magnification

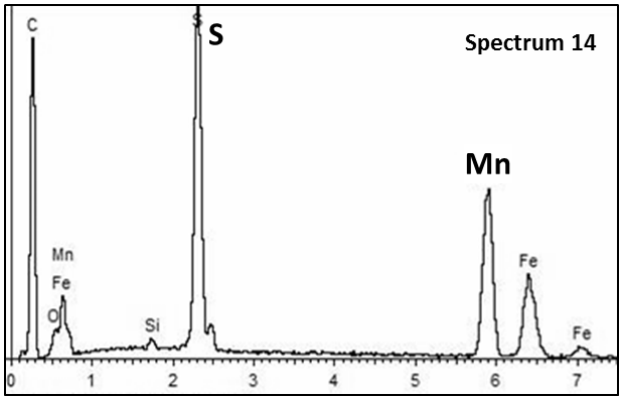

b) WDX/SEM spectrum of MnS

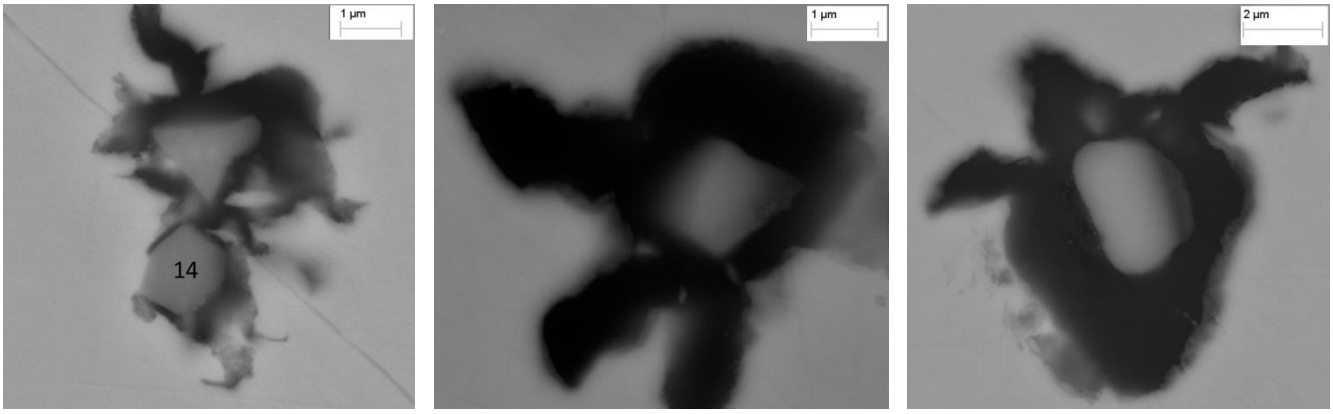

c) High magnification: graphite growing around MnS nuclei

Fig. 14. Nucleation of lamellar graphite in heat Q5LAG (0.12% S) in the early stage of solidification (f_S<0.35); non-etched.

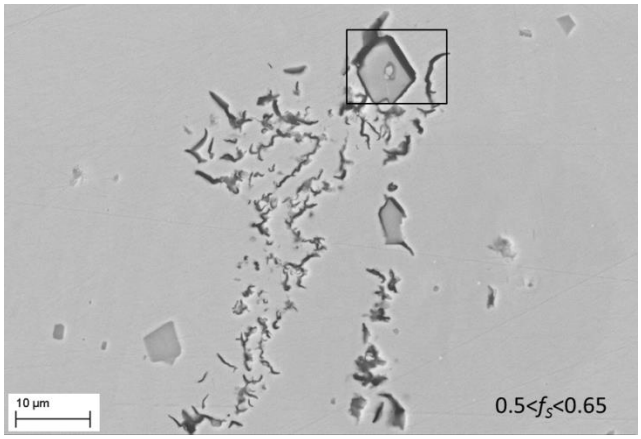

a) MnS inclusions acting as graphite nuclei

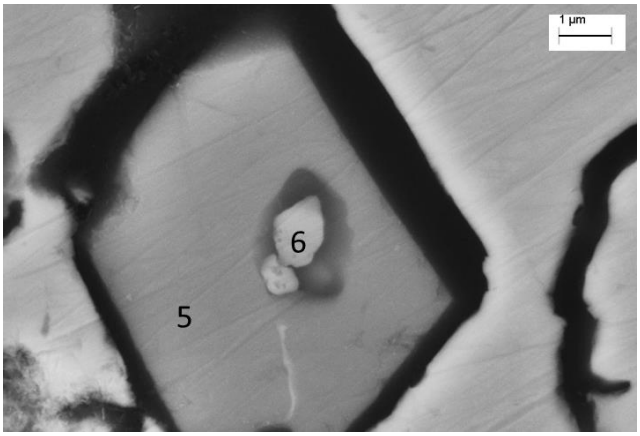

b) MnS nucleated on Zr, Al, Mn, Mg, Ca oxy-sulfide

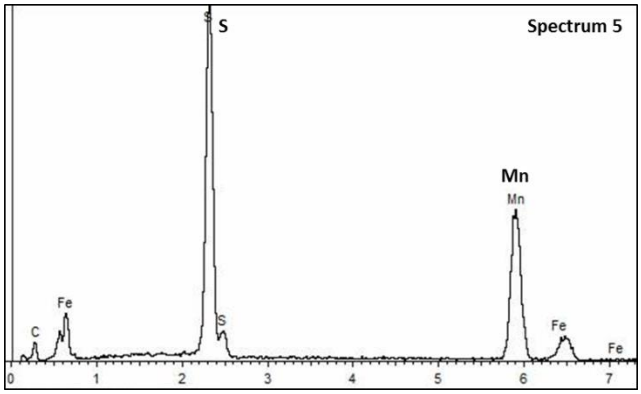

c) WDX/SEM spectrum of MnS

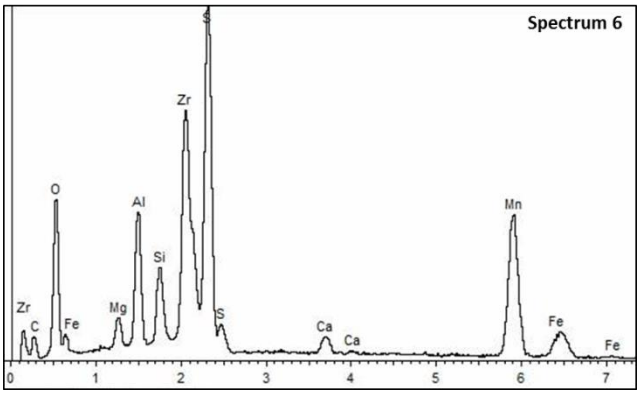

d) WDX/SEM spectrum of complex oxy-sulfide

Fig. 15. Nucleation and growth of lamellar graphite in heat Q5LAG (0.12% S) during later solidification (f_S>0.65); non-etched.

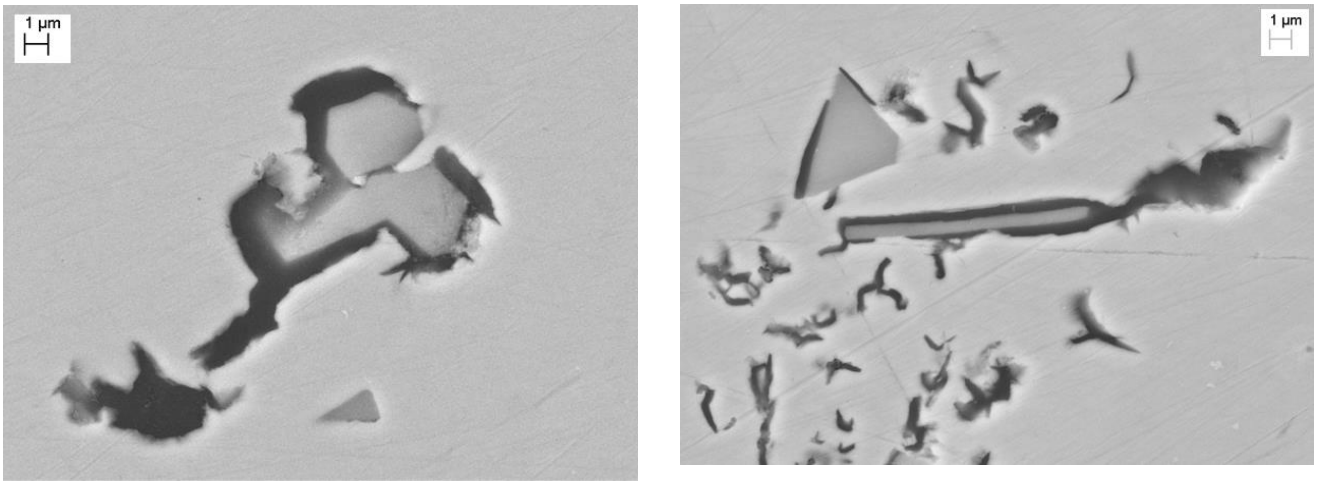

a) nucleation of graphite on polygonal MnS inclusions

b) nucleation of graphite on plate MnS inclusions

Fig. 16. Different shapes of MnS inclusions in heat Q5LAG (0.12% S); non-etched.

DISCUSSION

Form the experimental results presented in this work it is confirmed that in unalloyed very low sulfur irons (0.011% S) with high Mn/S ratio (51.8) interdendritic graphite type-D nucleates at the austenite/liquid interface where carbon rich regions are generated by carbon rejection from the solidifying austenite. As the sulfur content increases to 0.028% and the Mn/S ratio decreases to 19.6, most type-D graphite nucleation continues to occur at the γ/L interface. However, limited nucleation can also take place on MnS inclusions.

At high sulfur contents (0.12% S) and low Mn/S (4.4), both nucleation pattern and graphite shape change drastically. The MnS inclusions exhibiting a variety of shapes become the main source for lamellar type-A graphite nuclei. The graphite grows by first enveloping the inclusions and then branching out in the liquid. The manganese sulfides are in turn nucleated by complex oxy-sulfides, such as Zr, Al, Mn, Mg oxy-sulfides described in this paper, or Al, Mg, Si, Ca oxides outlined in some of our previous work[15], as well as by previous researchers[17].

The addition of titanium to the iron affects significantly both graphite shape and graphite nucleation. In the very low sulfur iron (0.011% S) the graphite changes from interdendritic type-D to superfine interdendritic SIG. While most of the graphite nucleation still occurs at the γ/L interface, some nucleation on cuboidal TiC was also observed.

Increasing the Ti level to 0.32% at the same sulfur content does not seem to produce significant other changes in the microstructure, with the exception of the formation of needle-like complex Ti-C-S-Mn compounds. It is not clear if these inclusions act as nuclei for graphite.

CONCLUSIONS

The purpose of this work was to investigate graphite nucleation in gray iron with various amounts of sulfur and titanium. Interrupted solidification (quenching) experiments were conducted on hypoeutectic gray irons with 0.011-0.12% S and 0.013-0.32% Ti. It was found that in low sulfur irons nucleation occurs mostly at the austenite/liquid interface where carbon –rich regions are formed because of rejection of carbon by the solidifying austenite. However, in some instances, nucleation occurred on cuboidal titanium carbides. Titanium additions change graphite shape from interdendritic to superfine interdendritic. Graphite nucleation is still mostly controlled by the sulfur level. In the high sulfur iron nucleation occurs on manganese sulfides, which nucleate on complex oxy-sulfides.

REFERENCES

1. Lux, B., *Giesserei Forschung*, 19, p. 141 (1967).
2. Geier, G.F., Bauer, W., McKay, B.J., Schumacher, P., *Mat. Sci. Eng*., A413-414, p. 339-345 (2005).
3. Larrañaga, P., Sertucha, J., Loizaga, A., Suarez, R., Stefanescu, D. M., *AFS Transactions*, Vol. 120, pp. 347-353 (2012).
4. Larrañaga, P., Sertucha, J., Loizaga, A., Suarez, R., Stefanescu, D. M., AFS Transactions, Vol. 120, pp. 337-346 (2012).
5. Okada, A., Miyake, H., "The Unknown World of Cast Iron (in Japanese)," KANSAI Univ. Press, p. 141 (1996).
6. Wilford, K.B., Wilson, F.G., *British Foundryman*, Vol. 78, pp. 301; 364 (1985).
7. Lux, B., *Recent Research on Cast Iron*, H.D. Merchant ed., Gordon and Breach p. 241 (1968).

8. Sun, G.X., Loper, C.R., AFS Transactions, Vol. 91, pp. 639-646 (1983).
9. Wallace, J.F., *AFS Transactions*, Vol. 83, pp. 363-378 (1975).
10. Francis, B., *Metallurgical Transactions A*, 10A (1979).
11. Riposan, I., Chisamera, M., Stan, S., Skaland, T., "Proceedings of the AFS Cast Iron Inoculation Conference," pp. 31-41 (2005).
12. Muzumdar, K.M., Wallace, J.F., *AFS Transactions*, Vol. 81, pp. 412-423 (1973).
13. Alonso, G., Stefanescu, D.M., Larrañaga, P., Sertucha, J., Suarez, R., *AFS Transactions*, Vol. 120, pp. 329-335 (2012).
14. Stefanescu, D.M., Alonso, G., Larrañaga, P. Suarez, R., *Acta Mater.*, Vol. 103, pp 103-114 (2016).
15. Moumeni, E., Stefanescu, D.M., Tiedje, N.S., Larrañaga, P., Hattel, J.H., *Metal. Mater. Trans. A*, 44A (11), pp. 5134-5146 (2013).
16. Alonso, G., Stefanescu, D.M., Larrañaga, P., De la Fuente, E., Aguado, E., Suarez, R., "Advances in the Science and Engineering of Casting Solidification," Nastac, L., Liu, B.C., Fredriksson, H., Lacaze, J., Hong, C.P., et al. eds., Wiley TMS, pp.347-354 (2015).
17. Riposan, I., Chisamera, M., Stan, S., Skaland, T., *Int. J. Cast Metals Res.*, 16 (1-3), pp. 105-111 (2003).